



**HAL**  
open science

# Myelin-induced gain control in nonlinear neural networks

Jérémie Lefebvre, Andrew Clappison, Longtin André, Axel Hutt

► **To cite this version:**

Jérémie Lefebvre, Andrew Clappison, Longtin André, Axel Hutt. Myelin-induced gain control in nonlinear neural networks. 2024. hal-04835140

**HAL Id: hal-04835140**

**<https://inria.hal.science/hal-04835140v1>**

Preprint submitted on 13 Dec 2024

**HAL** is a multi-disciplinary open access archive for the deposit and dissemination of scientific research documents, whether they are published or not. The documents may come from teaching and research institutions in France or abroad, or from public or private research centers.

L'archive ouverte pluridisciplinaire **HAL**, est destinée au dépôt et à la diffusion de documents scientifiques de niveau recherche, publiés ou non, émanant des établissements d'enseignement et de recherche français ou étrangers, des laboratoires publics ou privés.



Distributed under a Creative Commons Attribution 4.0 International License

1 Myelin-induced gain control in nonlinear neural  
2 networks

3 Jérémie Lefebvre<sup>1,2,3,4\*†</sup>, Andrew Clappison<sup>5</sup>, André Longtin<sup>2†</sup>,  
4 Axel Hutt<sup>6,7†</sup>

5 <sup>1</sup>\*Department of Biology, University of Ottawa, Ottawa, ON K1N 6N5,  
6 Ontario, Canada.

7 <sup>2</sup>Department of Physics, University of Ottawa, Ottawa, ON K1N 6N5,  
8 Ontario, Canada.

9 <sup>3</sup>Krembil Brain Institute, University Health Network, Toronto, ON  
10 M5T 0S8, Ontario, Canada.

11 <sup>4</sup>Department of Mathematics, University of Toronto, Toronto, ON M5S  
12 2E4, Ontario, Canada.

13 <sup>5</sup>School of Electrical Engineering and Computer Science, University of  
14 Ottawa, Ottawa, ON K1N 6N5, Ontario, Canada.

15 <sup>6</sup>Mimesis, Inria Centre at Université de Lorraine, Strasbourg, 67000,  
16 France.

17 <sup>7</sup>MLMS, Université de Strasbourg, CNRS, iCube, Strasbourg, 67000,  
18 France.

19 \*Corresponding author(s). E-mail(s): [jeremie.lefebvre@uottawa.ca](mailto:jeremie.lefebvre@uottawa.ca);  
20 Contributing authors: [aclap051@uottawa.ca](mailto:aclap051@uottawa.ca); [alongtin@uottawa.ca](mailto:alongtin@uottawa.ca);  
21 [axel.hutt@inria.fr](mailto:axel.hutt@inria.fr);

22 †These authors contributed equally to this work.

23 **Abstract**

24 Myelin surrounds axonal membranes to increase the conduction velocity of nerve  
25 impulses and thus reduce communication delays in neural signaling. Changes in  
26 myelination alter the distribution of delays in neural circuits, but the implica-  
27 tions for their operation are poorly understood. We present a joint computational  
28 and non-linear dynamical method to explain how myelin-induced changes in ax-  
29 onal conduction velocity impact the firing rate statistics and spectral response  
30 properties of recurrent neural networks. Using a network of spiking neurons with  
31 distributed conduction delays driven by a spatially homogeneous noise, combined

32 probabilistic and mean field approaches reveal that myelin implements a gain  
33 control mechanism, optimizing neural coding while stabilizing neural dynamics  
34 away from oscillatory regimes. The effect of myelin-induced changes in conduc-  
35 tion velocity on network dynamics was found to be more pronounced in presence  
36 of correlated stochastic stimuli. Further, computational and theoretical power  
37 spectral analyses reveals a paradoxical effect where the loss of myelin promotes  
38 oscillatory responses to broadband time-varying stimuli. Taken together, our find-  
39 ings show that myelination can play a fundamental role in neural computation  
40 and its impairment in myelin pathologies such as epilepsy and multiple sclerosis.

41 **Keywords:** Myelin, Delays, Recurrent networks, Computation, Nonlinear dynamics,  
42 Noise, Mean-field

43 Nonlinear systems with delayed feedback have widespread applications across the fields  
44 of physics[1], engineering [2] and biology [3]. In biological neural networks, time delays  
45 reflect the combined effect of slow synaptic transmission and the finite propagation  
46 velocity of nerve impulses along axons. Moreover, delayed neural signaling has been  
47 shown to support a wide range of nonlinear phenomena in the brain, ranging from  
48 collective synchronization [4, 5], stochastic resonance [6] and induction of brain oscil-  
49 lations [7] to various types of noise-induced bifurcations [8–13]. For this reason, time  
50 delays have been implicated with a rich repertoire of physiological dynamics support-  
51 ing brain function [12, 14–16].

52 In the nervous system, axonal conduction delays are not free parameters but are  
53 strictly regulated by myelin, a fatty substance enwrapping neural membranes. Myelin  
54 enables saltatory conduction, and greatly accelerates the propagation of action po-  
55 tentials (APs) along axons. Produced by glia cells, myelin compensates for variability  
56 in length and caliber between different axons [17–19], adjusting the time required for  
57 APs to propagate towards their post-synaptic targets (known as conduction delay).  
58 Conduction delays are of prime importance for the faithful transmission of corre-  
59 lated and/or temporally structured fluctuations resulting from recurrent connectivity  
60 [20, 21], sensory stimuli and/or functionally relevant afferent inputs. Such correlated  
61 stimuli challenge both the limited coding capacity of neurons[22], as well as the tem-  
62 poral coordination of neural signaling [17, 19, 21, 23]. To face this challenge, glial cells  
63 can adaptively adjust the amount of myelin along axons, speeding up or slowing down  
64 the propagation of APs by tuning conduction velocity, thereby stabilizing neuronal  
65 trafficking [12, 13, 24–27]. Indeed, myelin has recently been shown to be plastic, sup-  
66 porting and imparting flexibility for various neural computations, notably by opimizing  
67 conduction delay distributions amongst neuronal assemblies [27–31] with important  
68 consequences on neural dynamics, synchrony and brain function[13, 21, 27, 32, 33].  
69 Research on glial cells, especially myelin, has emerged as one of the most effervescent  
70 and rapidly evolving areas in neuroscience (see [34] and references therein).

71 In the light of the manifest richness of delayed feedback systems [3], it is no sur-  
72 prise that myelin-induced changes in axonal conduction velocity (and delays) influence  
73 neural signaling and transform the dynamics of neural circuits and how they respond  
74 to time-varying fluctuations. Yet, networks with time delays are amongst the most

75 challenging to characterize mathematically, which severely limits data interpretation.  
76 We here explore this problem using a spiking neural network of excitatory neurons,  
77 with distributed delay and correlated additive noise. In our analysis, we considered  
78 conduction velocities over a range aligned with experimental observations made in the  
79 central nervous system of across multiple mammalian species [19, 35, 36].

80 We develop a computational strategy for stochastic spiking networks, and associ-  
81 ated non-Markovian theory, that lifts the restriction of single delays to reveal a host of  
82 new delay density-dependent dynamical phenomena of physiological and clinical rele-  
83 vance. Leveraging mean field theory, we develop a method to determine the statistics  
84 of the stationary probability density function associated with the collective neuron  
85 activity in this network. Building on previous results on stochastic delay equations  
86 [37–41], this approach permits the derivation of implicit expressions for statistical mo-  
87 ments of the mean field dynamics. Most importantly, it reveals that delay distributions  
88 may regulate the activity of cells in these network by tuning their individual dynamic  
89 range and encoding capability for noise-like stimuli. Using this approach, we charac-  
90 terize changes in neural activity resulting from variation in axonal conduction velocity  
91 reflecting various levels of myelination.

92 While it is generally assumed that delays mainly influence synchrony and oscilla-  
93 tions, our mathematical and numerical results show that myelin-induced changes in  
94 conduction velocity implement a gain control mechanism amplifying neural activity,  
95 independently of synaptic coupling, and/or irrespective of the presence of oscillations.  
96 This gain control mechanism was further found to be especially salient in the presence  
97 of dynamic stimuli by amplifying the collective response of the neurons to time-varying  
98 signals. Changes in conduction velocity were found to shape the information coding  
99 capacity of the network, suggesting that myelination may be tuned in a contextual  
100 way to optimize the faithful encoding of stimuli of a given amplitude and baseline  
101 noise into network firing properties [21, 42]. In addition, power spectral analysis re-  
102 veals that the dispersion of time delays, resulting from either variability in conduction  
103 velocities and/or axonal lengths, regularizes neural activity, suppressing oscillatory  
104 activity and promoting asynchronous dynamics. These findings echo effects seen ex-  
105 perimentally under the influence of activity-dependent myelination [17, 24, 26, 27, 29].  
106 Taken together, these results allow us to draw conclusions about how myelination may  
107 solicit nonlinear neural interactions to implement gain control and optimize the en-  
108 coding capability of neural circuits. Further, they enable us to make predictions about  
109 potential dynamical consequences of myelin disruption in pathological states, such as  
110 those seen in epilepsy [43] and/or multiple sclerosis[44].

## 111 Results

112 Our analysis starts with the observation that the collective activity of neurons in our  
113 network model (cf. Methods section) is highly sensitive to myelination. Exposing in-  
114 dividual neurons to a spatially correlated stimuli, a consistent increase in the mean  
115 network firing rate could be observed whenever conduction velocity - reflecting myeli-  
116 nation - is increased. As shown in Fig. 1, faster conduction was found to amplify neural  
117 activity and firing rates, and the network response to stimuli became more salient,

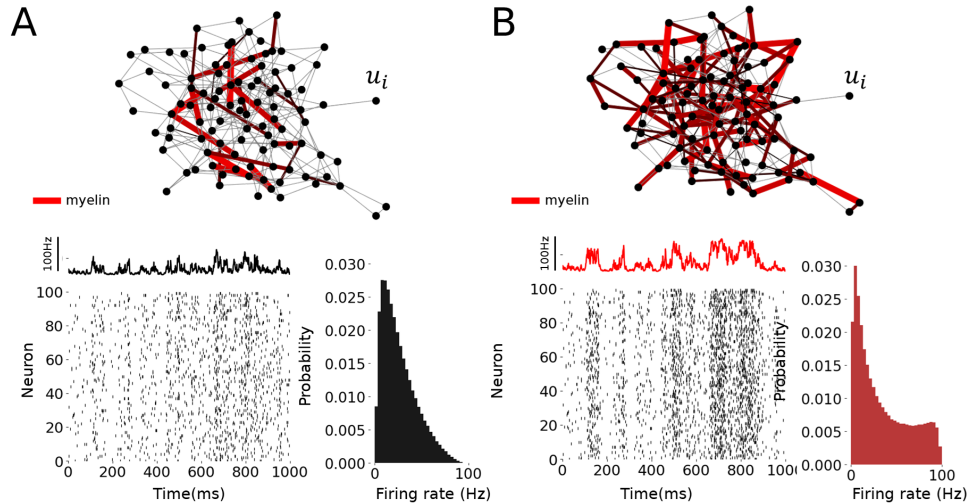


**Figure 1 Gain control induced by axonal conduction velocity** **A**. Network of Poisson spiking neurons with low ( $c = 0.5\text{m/s}$ ) conduction velocity, reflecting poor myelination. The diagram illustrates neurons (black circles) connected through axons (edges) expressing different conduction delays due to various degrees of myelination (illustrated in shades of red). A raster plot of the network spiking activity shown alongside the network mean firing rate above shows the response of the network to a spatially correlated stochastic stimulus  $S(t)$ . The histogram corresponds to the firing rate distribution of the network (right insert). **B** For the same stimulus  $S(t)$ , if conduction velocity is increased ( $c = 50\text{m/s}$ ) to reflect higher myelination, the response of the network is amplified and mean firing rates increase. This also manifests as a change in the network firing rate distribution, which is now heavily skewed (right insert). In **A** and **B**, axonal conduction delays  $\tau_{ij} = l_{ij}/c$  are Gamma distributed with shape  $k = 2$  and scale  $\theta = 4/c$  ms and axonal length distribution  $l_{ij}$ . Except from conduction velocity (i.e.,  $c$ ), all other parameters are identical. The network is fully (i.e., all-to-all) connected and synaptic weights are both positive and identical. The other parameters in the model (cf. Methods section) used for these exemplar simulations are  $N = 100$ ,  $J_{ij} = \bar{J} = 0.9$ ,  $I = 0$  and  $D = 0.05$ . The activation function is nonlinear with parameters  $\beta = 2$ ,  $h = 0.5$ .

118 suggestive of a gain control effect. We note that this effect is entirely due to a shift  
 119 in delay distribution within the network: aside from conduction velocity, all other pa-  
 120 rameters - such as synaptic weights - were kept constant. The presence of this response  
 121 amplification could also be confirmed by computing the network mean firing rate distri-  
 122 bution, where faster conduction promotes increased probability of high firing rates  
 123 (see below).

## 124 Mean field statistics

125 To better understand this phenomenon, we examined how conduction velocity (i.e.  
 126  $c$ ), reflecting the amount of myelin covering axons, shapes the dynamical properties  
 127 of cells in the network. This was accomplished by computing the probability density  
 128 function of the network-averaged instantaneous potential  $\bar{u}$ , a quantity that fluctuates  
 129 in time as determined by the network collective dynamics. This was done for two dif-  
 130 ferent categories of delay distributions: Gamma, and uniformly distributed. This was

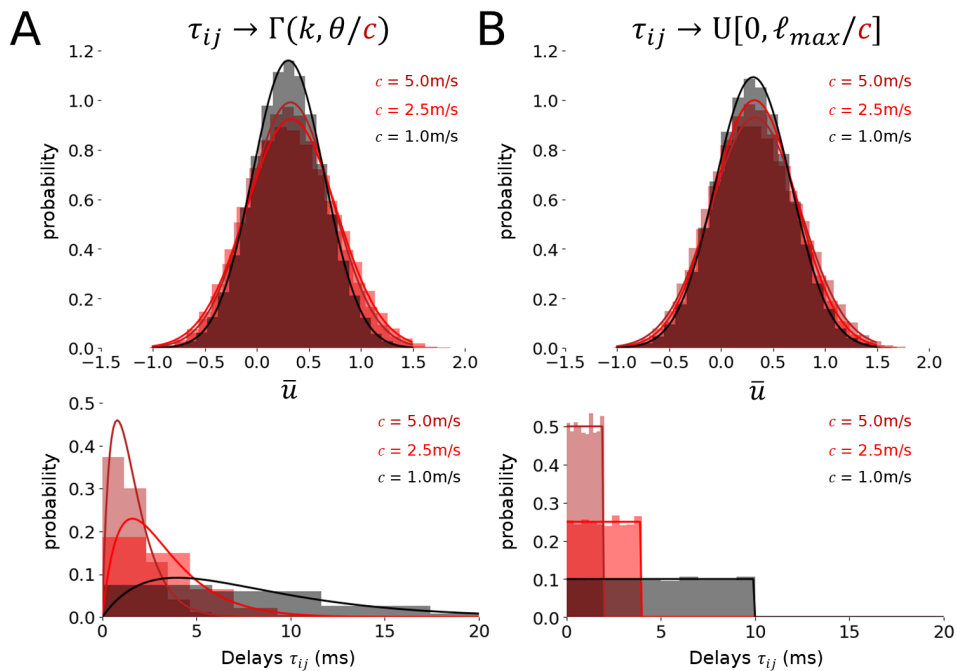


**Figure 2 Axonal conduction velocity shapes delay distributions and corresponding mean field statistics** **A** Mean field probability density function (top) computed numerically for a network of spiking neurons with Gamma-distributed delays (bottom). The mean field probability density function may be well approximated by a Gaussian (solid lines), and its mean and variance changes as conduction velocity increases. The associated delay distributions are plotted alongside their analytical probability distributions. Here, the shape parameter is  $k = 2$  and the scale  $\theta = 4/c$  ms. **B** Corresponding mean field distribution for uniformly distributed delays (top) and associated delay distributions (bottom). Here,  $l_{\max} = 10$ mm. Numerical simulations [45] of the network ensemble average  $\bar{u}$  (shaded areas) are shown alongside normal distributions with associated mean and variance (curves) for  $c = 5.0$  m/s (dark red),  $c = 2.5$  m/s (red) and  $c = 1.0$  m/s (black), respectively. Simulations were performed using the Euler-Maruyama scheme, with a population of  $N = 100$  neurons over trials of duration  $T = 500$ s with steps of 1ms and  $D = 0.1$ . Other parameters are  $J_{ij} = \bar{J} = 0.9$ ,  $I = 0$ , and the activation function is nonlinear with parameters  $\beta = 2$ ,  $h = 0.5$ .

131 first computed numerically through simulations (see Subsection *Mean Field Moments*  
 132 in the Methods section for details of the mathematical analysis), which then motivated  
 133 our theoretical work. Within the range of parameters examined here, Fig. 2 indicates  
 134 that the probability density function of the network mean may be well approximated  
 135 by a Gaussian - a feature that unlocks a variety of properties that makes this prob-  
 136 lem amenable to a thorough analytical characterization. These simulations also reveal  
 137 changes in mean field statistics: increasing the conduction velocity increases both the  
 138 mean and variance of the network mean potential, or conversely, larger conduction  
 139 delays tend to suppress both the mean and variance of the network mean activity.

140 As a consequence of this Gaussian property, high-order moments of the probability  
 141 density function (i.e.,  $\rho_S(\bar{u})$ ) can be assumed to be small, so that the mean field  $\bar{u}$  in

Eq. (2) may be used to develop equations for the dynamics of the mean (i.e.,  $\mu$ ) and variance (i.e.,  $\sigma^2$ ). This allows the derivation of the stationary distribution without relying on a Fokker-Planck formalism [38, 40, 41, 46]. We used this strategy to compute the stationary mean and variance of the mean field and characterized their respective dependence on myelin - that is, on conduction velocity and resulting delay distribution - and on the noise variance  $D$ . As shown in Fig. 3A-B for both Gamma- and uniformly distributed delays, conduction velocity increases both the mean and variance of the mean field  $\bar{u}$ , confirming the numerical observations in Figs. 1 and 2. While the changes in mean and variance induced by faster conduction velocity portrayed in Fig. 3 might appear small, they in fact support significant variations in mean firing rate (see Fig. 1 and below). We could further confirm the alignment between our analytical derivations and analytical results, which were found to be in good agreement over multiple orders of magnitude of the noise amplitude. We note that deviations between our analytical and numerical results were however observed for higher values of the noise variance, as the system approaches a regime characterized by stochastic/coherence resonance [21, 47]. However, it is interesting to note that the theoretical predictions for the variance were accurate over a broader range of noise variance compared to the mean.

The changes in statistics portrayed in Figs. 1-3 together with our theoretical analysis suggest that myelination impacts the recurrent interactions of the network by modulating neural activity and increasing the saliency of stimuli through augmented responses. This results directly from the expression of mean field moments. Notably, the stationary variance  $\sigma_s^2$  is shown to scale with both the stimulus amplitude  $D$ , and the summed contribution of delay-dependent correlations  $C_k$  in mean potential measured across the network (see Methods section; Eq. (9)). As conduction velocities are decreased, these delay-dependent correlations are suppressed: the network behaves as if it was effectively disconnected (i.e.,  $\sigma_s^2 = D$ ). Consequently, by increasing conduction velocity, myelination solicits recurrent interactions in the network, promoting correlated activity and amplifies the temporal coordination between cells. We note that this gain effect occurs here because the network is purely excitatory (see Discussion).

## Gain control and susceptibility depend on conduction velocity

Taken together, the above results suggest that neural networks may utilize changes in myelination and axonal conduction velocity, as well as resulting shifts in activity portrayed in Fig. 3, to optimize the representation of information about stimuli - such as noise variance and bias - which in turn could be favorably read out by a downstream network. Indeed, as we now show, the variance  $D$  of the spatially correlated noise input and the input strength  $I$  influence network firing statistics and sensitivity to these variables in a manner that is contingent on the distribution of delays between neurons, and specifically, on the mean conduction velocity. The aforementioned changes in stationary mean and variance of the network ensemble average  $\bar{u}$  in Fig. 3 may hence be recast as the manifestation of a gain control effect, in which the saliency of neuronal responses can be amplified through adjustments in axonal conduction velocity [21].

To characterize the dynamic range and sensitivity of the network, we computed the susceptibility or gain  $G$  of the network for different conduction velocities. This susceptibility quantifies how the mean firing rate changes with the noise variance (i.e.  $D$ ) or

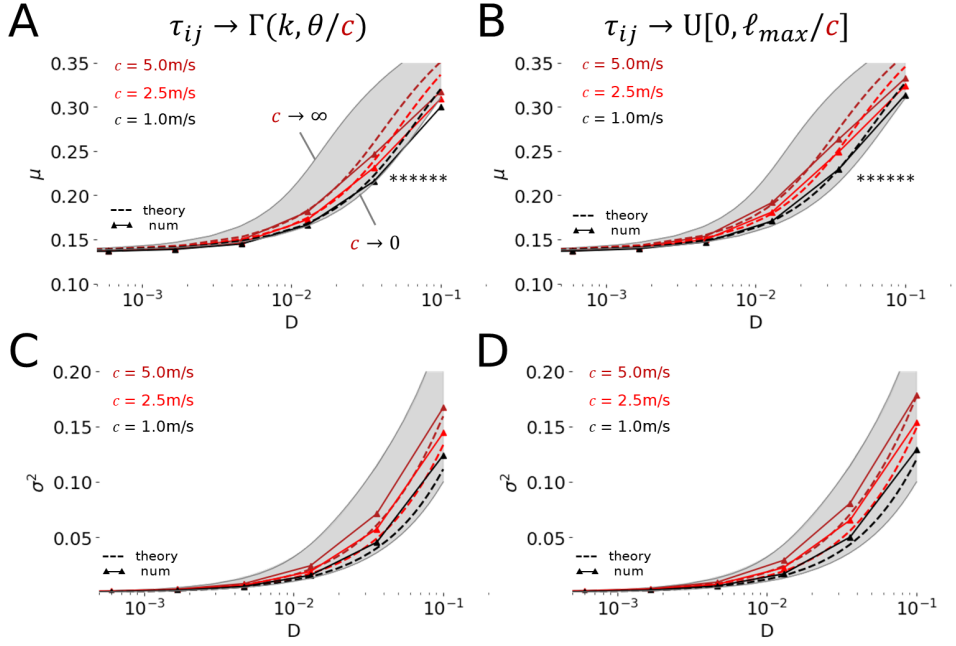


**Figure 3 Mean field stationary statistics.** **A** Stationary mean of the network ensemble average  $\bar{u}$  computed numerically (triangles) plotted alongside the stationary mean  $\mu_S$  computed analytically (dotted lines, see Methods section Eqs. (18), (22)) for Gamma distributed delays, and across various conduction velocities considered ( $c = 5.0\text{m/s}$ , dark red;  $c = 2.5\text{m/s}$ , red;  $c = 1.0\text{m/s}$ , black) and various orders of noise variances  $D$ . The grey shaded area is bounded by the limit cases where there are no delays (top,  $c \rightarrow \infty$ ) or alternatively if delays become infinite (bottom,  $c \rightarrow 0$ ). Both of these limits were computed analytically. Significant deviations between numerical and analytical results emerge for strong noise variances  $D$  (marked by stars). **B** Equivalent plot for uniformly distributed delays. **C** Stationary variance (i.e.,  $\sigma^2$ ) of the network ensemble average  $\bar{u}$  for Gamma distributed delays, computed both numerically (triangles) and analytically (dotted lines), see Methods section for details. Here, deviations appear for large noise variances  $D$  (marked as stars). **D** Same as panel **C** for uniformly distributed delays. In panels **A** and **C**,  $k = 2$  and  $\theta = 4\text{mm}/c$ . In panels **B** and **D**,  $l_{\max} = 10\text{mm}$ . Simulations were performed using the Euler-Maruyama scheme, with a population of  $N = 100$  neurons over trials of duration  $T = 500$  secs with steps of 1ms. Other parameters are  $J_{ij} = \bar{J} = 0.9$ ,  $I = 0$ , and the activation function is nonlinear with parameters  $\beta = 2$ ,  $h = 0.5$ .

186 the constant input strength (i.e.  $I$ ) for different values of  $c$ . This gain corresponds to  
 187 the slope of the network activation function  $F$  averaged over the probability density  
 188 of the mean potential (cf. Eq. (21) in the Methods section). We remind here that as  $D$   
 189 is swept across the shown range, the values of the mean  $\mu_S$  and variance  $\sigma_S$  have to  
 190 be continually and self-consistently recomputed in order to evaluate the gain function.

191 As can be seen in Fig. 4A, the mean firing rate scales monotonically with noise ampli-  
 192 tude, as one intuitively expects. Moreover, as conduction velocity  $c$  increases, the  
 193 mean firing rates of the individual neurons - and thus of the whole network - increase  
 194 as well, a direct consequence of the phenomenon portrayed in Fig. 3. We note that  
 195 despite seemingly small changes in mean membrane potential (i.e., Fig. 3), firing rates

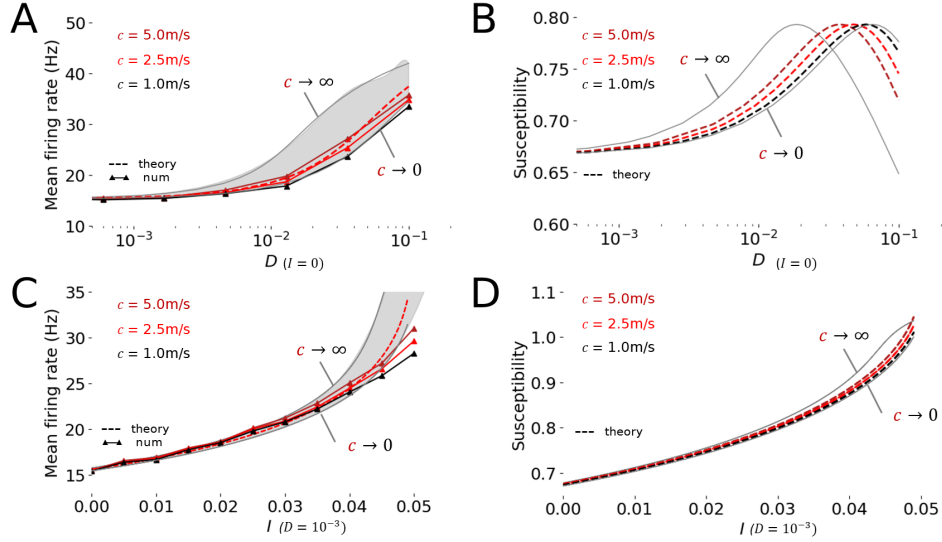


**Figure 4 Delay-induced firing and gain control as a function of noise and input strength.** **A** Mean network firing rate as a function of noise variance  $D$  for various axonal conduction velocities ( $c = 5.0\text{m/s}$ , dark red;  $c = 2.5\text{m/s}$ , red;  $c = 1.0\text{m/s}$ , black). Firing rates are computed by multiplying the network firing probability  $F$  by a factor of 100. These rates expectedly scale with  $D$ , but are also amplified by higher conduction velocity. The grey shaded area is bounded by the limit cases where there are no delays (top,  $c \rightarrow \infty$ ) or alternatively if delays become infinite (bottom,  $c \rightarrow 0$ ). Both of these limits were computed analytically. The theory (dashed line) agrees well with the simulation of the full spiking network. **B** Network gain  $G$  or susceptibility as a function of  $D$  for different conduction velocities. These theoretical curves represent the slope of the curves in (A), and reveal an optimal noise strength that decreases with conduction velocity. Grey lines represent the same cases as in panel A. **C** Mean firing rate as a function of constant input strength  $I$  for different values of  $c$ . Theory (dashed line) is accurate up to approximately  $I=0.045$ , after which discrepancies grow due to the nonlinear behaviour of the network and the fact that the theory does not account for increased spiking noise variance in the network simulations. **D** Susceptibility as a function input strength  $I$  for different  $c$  values. The theory is accurate again over the same range as in C. Network simulations for higher values of  $I$  reveal a susceptibility peak due to the inflection point present in panel C. The model assumes a distribution of axonal lengths and delays are Gamma-distributed with  $k = 2$  and  $\theta = (4\text{mm}/c)$ . Other parameters are  $\bar{J} = 0.9$ , and the activation function is nonlinear with parameters  $\beta = 2$ ,  $h = 0.5$ .

196 experience important changes, increasing by about 20% as conduction velocity is in-  
 197 creased from 1m/s to 5m/s, and even more if conduction velocity is increased further.

198 Such gain control effect must however be regarded from the perspective of the neu-  
 199 rons' limited dynamic range and coding capacity: stimuli that are too weak may fail  
 200 to elicit a visible postsynaptic response in terms of network firing rate. If their ampli-  
 201 tude is too strong, such stimuli may in contrast lead to saturation (i.e., postsynaptic  
 202 neuron fires continuously). As direct manifestation of this, Figure 4B shows that the  
 203 gain peaks as a function of the noise strength, and this peak shifts to smaller values  
 204 of  $D$  as the velocity increases. This indicates that while myelin might control the re-  
 205 sponse gain, it is the stimulus amplitude  $D$  that dictates whether the susceptibility is

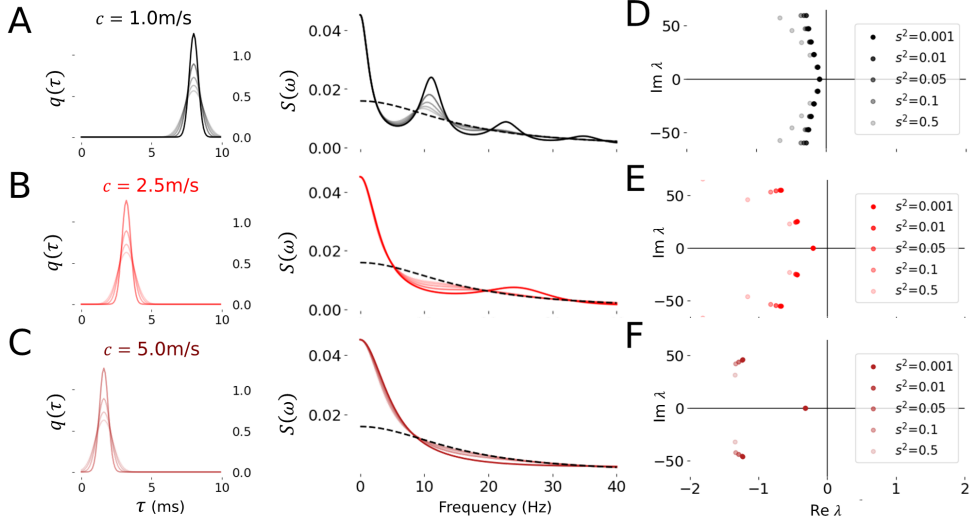


**Figure 5 Stabilizing effect of delay variability.** **A-C** Gaussian delay distributions (left) determine the shape of the mean field power spectral density  $S(\omega)$  (right). The Gaussian mean and variance are independent from each other. Here, the mean delay is kept constant and given by  $m = k\theta/c$ , while the variance is increased from  $s^2 = 0.001$  to  $0.5$  (lines with increased shading). To compute the power spectral density, we assumed a stimulus  $S(t)$  with noise variance  $D = 0.05$  and zero bias i.e.,  $I = 0$ . The dashed line corresponds to the Lorentzian power spectral density associated with  $\bar{J} = 0$ . Increasing the conduction velocities shifts the mean delay, and are given by  $c = 1.0 \text{ m/s}$  (black lines, panel **A**);  $c = 2.5 \text{ m/s}$  (red lines, panel **B**);  $c = 5.0 \text{ m/s}$  (dark red lines, panel **C**). **D-F** Eigenvalues associated with the characteristic polynomial (cf. Eq. (26) in the Methods section) whenever conduction velocity  $c$  is fixed and the delay variance  $s^2$  is varied. Increasing the delay dispersion  $s^2$  shifts the oscillatory eigenvalues away from the imaginary axis and stabilizes the dynamics. Different conduction velocities are given by  $c = 1.0 \text{ m/s}$  (black shading, panel **D**),  $c = 2.5 \text{ m/s}$  (red shading, panel **E**) and  $c = 5.0 \text{ m/s}$  (dark red shading, panel **F**). Other parameters are  $\bar{J} = 0.9$ ,  $k = 2$ ,  $\theta = 4 \text{ mm}$ ,  $I = 0$ , and the activation function is nonlinear with parameters  $\beta = 2$ ,  $h = 0.5$ .

206 increased or decreased over the neurons dynamic range. This suggests that myelination  
 207 may be tuned in a contextual way to optimize the faithful encoding of stimuli of  
 208 a given amplitude and baseline noise into network firing properties [21, 42].

209 Figure 4C shows the corresponding results when the (constant) input bias (i.e.,  $I$ )  
 210 is increased. While the mean firing rate expectedly changes as  $I$  is increased, the ef-  
 211 fect of conduction velocity and/or delay distribution does not appear to impact the  
 212 response significantly compared to the noise strength  $D$ . The same trend can be seen  
 213 in Fig. 4D, where the susceptibility monotonically increase with input strength but  
 214 does not vary significantly with conduction velocity. These observations suggest that  
 215 conduction velocity mainly influences the response of the network to dynamic, time-  
 216 varying stimuli and not constant inputs.

217 These observations together suggest that conduction velocity may be tuned in a  
 218 contextual way to optimize the faithful encoding of stimuli into network firing prop-  
 219 erties [21, 42]. We further note the good agreement of our theory with the numerical  
 220 simulations of the spiking network, but only as long as  $I$  does not exceed the range

221 shown. Beyond that, the susceptibility also peaks, albeit with a relative invariance to  
222 conduction velocity. We hypothesize that this is due to the system being pushed into  
223 a more nonlinear regime, in particular one in which neglecting the increase in Pois-  
224 son noise leads to a substantial error. Coherence resonance may further amplify this  
225 discrepancy (see below).

## 226 Conduction delay variability stabilizes network dynamics

227 We concluded our study by examining the effect of delay dispersion on the response  
228 of our network to time-varying stimuli. To do so, we computed the power spectral  
229 density  $S(\omega)$  of the mean field  $\bar{u}$  for various delay distributions. For that purpose,  
230 we first relaxed our previous assumption by which eigenvalues associated with the  
231 dynamics of our network are purely real. We examined purely stochastic inputs (i.e.  
232 setting  $I=0$ ) and deliberately considered a limit case in which the delay distribution  
233 can be approximated by a Gaussian, so that the mean and variance may be modu-  
234 lated independently from one another (see Methods section *Power spectral density*).

235 As can be seen in Fig. 5A-C, increasing the mean delay - i.e., decreasing the degree  
236 of myelination and thus the conduction velocity - expectedly introduces resonant os-  
237 cillatory modes in the network, whose frequencies scale with conduction velocity. Such  
238 frequencies can easily be determined through linear stability analysis, corresponding  
239 to imaginary eigenmodes. Increasing the variance of the delay distribution (while  
240 keeping the mean delay constant) suppresses these resonances, as the power spectral  
241 density converges towards a purely Lorentzian distribution  $S(\omega) = D (\pi(1 + \omega^2))^{-1}$ .  
242 We highlight that the latter corresponds to the uncoupled case where  $J_{ij} = 0$ , in  
243 which the mean field in Eq. (23) simplifies to a non-delayed Langevin equation. To  
244 better understand the mechanism at play, we performed linear stability analysis of our  
245 mean field system, computing explicitly the eigenvalues and how they depend on con-  
246 duction velocity and delay variance (see Eq. (26)). As shown in Fig. 5D-F, increasing  
247 the dispersion of the delays while keeping their mean constant shifts complex eigen-  
248 value away from the imaginary axis. This indicates that delay dispersion quenches  
249 the oscillatory modes of the system, making the system increasingly linear. These ob-  
250 servations echo previous findings [48–50] showcasing the strongly stabilizing influence  
251 of delay dispersion, by which the system becomes effectively decoupled through the  
252 suppression of oscillatory modes, thereby promoting irregular, asynchronous activity.  
253

## 254 Discussion

255 The influence of time delays on nonlinear stochastic systems has been thoroughly  
256 studied [38, 40, 41], especially from the perspective of synchrony [48, 51, 52], yet their  
257 consequence on the computational properties of neural networks has received compar-  
258 atively less attention. Action potential conduction velocity is strongly influenced by  
259 the presence (and amount) of myelin covering the axon, which impacts the temporal  
260 coordination of neural signaling with important consequences on network dynamics  
261 [13, 18, 19, 21, 27, 29]. Glial-mediated changes in conduction velocity along axons have  
262 been shown to be titrated autonomously to promote AP coincidence [17], reinforcing

263 the probability of post-synaptic response and hence to enhance information transfer  
264 [21, 53] as well as the resilience of brain function [13, 26]. We leveraged mean field  
265 theory for stochastic delay equations [47, 54–56] to investigate how conduction veloc-  
266 ity - through its influence on conduction delays - influences the activity of recurrent  
267 networks and response to stimuli, in order to unveil the potential functional role of  
268 myelin in neural computations.

269 Using mean field theory, we analyzed an excitatory network of spiking neurons  
270 with distributed delay and additive, spatially correlated stimuli. The shape of the de-  
271 lay distribution in this network was allowed to change with conduction velocity, meant  
272 to reflect the net effect of myelin on AP propagation. Building on a set of assumptions  
273 supported numerically, we derived the stationary moments for the probability density  
274 function of the network ensemble average. Considering these delay distributions, we  
275 quantified the mean response of the network and its variability to changes in stimulus  
276 bias and noise strength. This analysis revealed that conduction velocity - through its  
277 effect on delay distribution - operates as a gain control mechanism, amplifying network  
278 firing rates to shared (correlated) input. Indeed, faster conduction velocity decreases  
279 delay dispersion (i.e., rendering conduction delays more similar to each other), in-  
280 creasing correlations in neural activity and, consequently, network firing rates. The  
281 network gain (i.e. susceptibility) was found to exhibit a peak as a function of noise  
282 strength as well as input strength, revealing that conduction velocity may be tuned to  
283 optimize the response of the network to these changes. Further, short delays, i.e. slow  
284 conduction, was found to promote oscillatory activity in the recurrent network. Our  
285 theory reproduces the gain properties seen in our numerical simulations of the spiking  
286 network, provided that the system is not pushed too far into its nonlinear regime.

287 Taken together, our computational and theoretical results suggest that myelinating  
288 glia in even simplified recurrent neural networks can play an important role in con-  
289 trolling firing rate statistics, along with their sensitivity to input changes beyond the  
290 induction of oscillations. Factoring in delay distributions also expands our knowledge  
291 about the determinants of firing rate distributions measured in real neural systems  
292 [57, 58]. Over the past decades, there has been a surge of interest in understanding  
293 the role played by myelin in brain function, health and disease [26, 27, 30, 59–61].  
294 Oligodendrocytes have since been implicated with a plethora of biological functions  
295 across the CNS, ranging from learning, memory consolidation, stimulus discrimina-  
296 tion to functional resilience [13, 28, 31–33, 59, 61, 62]. Yet, understanding how myelin  
297 - and by extension glia - shape the computational properties of neural networks re-  
298 mains a formidable challenge, notably because of the complexity of non-linear delayed  
299 feedback systems.

300 In light of these results, both insufficient and excessive conduction velocity (i.e.,  
301 myelination) represent potential disruptors of neural function. Recent experiments  
302 have causally linked excessive myelination to seizures in mice models of generalized  
303 epilepsy[43]. The gain control effect described here may thus be involved in supporting  
304 pathologically high firing rates and correlated neural activity, both of which accom-  
305 pany seizures [63]. Conversely, our model also predicts that decrease in conduction  
306 velocity predisposes the network to lower firing rates and gain, which may be associ-  
307 ated with impairments observed in demyelinating diseases such as multiple sclerosis

308 (MS) [28, 44, 64–67].

309 Our results are an extension to the distributed delay case of previous theoretical  
310 work on oscillations in single delay rate-based models with finite-size, spatially uncor-  
311 related noise [68], as well as in leaky integrate-and-fire stochastic networks without  
312 [69] and with [70] spatial noise correlations. Although our work has considered that  
313 the delay distribution resulted from a distribution in axonal lengths, the theory can  
314 not distinguish this case from that where the delay distribution arises due to changes  
315 in axonal diameters but fixed lengths, since it is known experimentally [19] that the  
316 axonal conduction velocity is proportional to axonal diameter for myelinated fibers.  
317 The more realistic situation may involve both significant diameter and length varia-  
318 tions, which could be taken into account in our theory.

319 Our approach suffers from limitations which should be developed in future studies.  
320 First, the network model considered here is purely excitatory. Future work addressing  
321 the impact of inhibition on our results is of great interest. How conduction velocity  
322 along both excitatory and inhibitory axons influences the dynamics of such networks  
323 would provide important information about the functional role of myelin, especially  
324 given excitatory and inhibitory neurons are known to display different myelination  
325 profiles [71, 72].

326 Moreover, we have introduced variability in conduction delays by sampling ax-  
327 onal lengths from a given probability (i.e., either Gamma or uniform) distribution,  
328 while keeping conduction velocity the same for all network axons. However, myelin  
329 distribution, caliber and/or g-ratio may vary along and between axons. Including this  
330 additional source of variability would lead to axon-specific conduction velocities. We  
331 note that, however, that resulting conduction delays would remain distributed - and  
332 hence the current results would remain qualitatively unaffected.

333 The network under study and associated mean field (see Methods section) are  
334 known to exhibit oscillations and/or stochastic/coherence resonance [21, 47, 51, 52, 54–  
335 56, 73]. Such dynamics yield non-Gaussian probability density profiles, and are further  
336 characterized by complex correlation rates  $\gamma$ . As such, our approach hold for positive  
337 values of synaptic weights ( $\bar{J} > 0$ ) below the multistability threshold, as well as for  
338 small values of the response gain  $\beta$  and noise amplitude  $D$ . We have also used a small  
339 delay expansion [41] to approximate the correlation rate  $\gamma$ , which would otherwise be  
340 both complex and satisfy a transcendental equation, greatly complicating the analysis.  
341 Despite this approximation, we highlight that our analysis remains in good agreement  
342 with the numerical simulations.

343 In addition, our network is fully connected (i.e., all-to-all) which was done for  
344 simplicity. We orient the reader to [21], where a similar network was examined with  
345 sparse connectivity. In our mean field equation (Eq. (2) in the Methods section), we  
346 have neglected fluctuations in membrane potential resulting from Poisson spiking.  
347 Such random fluctuations, whose amplitude scale with firing rate, have a multiplica-  
348 tive effect on the dynamics of Eq. (1) and may have profound influence on network  
349 stability [37]; it likely explains the limitation of our theory at high input strength.  
350 We hypothesize that this additional source of variability might be involved in the de-  
351 viations observed for high noise intensity in Fig. 3A-B. Lastly, our model is abstract  
352 and neglects multiple relevant physiological details in order to preserve mathematical

tractability. Further work is required to augment the biological accuracy of our model and its ability to mimic real brain circuits and the influence of glia on neural function.

## Methods

### Model

We considered a generic and widely used class of spiking recurrent neural networks in which the potential  $u_i$ ,  $i = 1 \dots N$ , of neurons is governed by the set of stochastic delayed equations with additive correlated noise

$$\tau_s \frac{d}{dt} u_i = L[u_i] + \frac{1}{N} \sum_{j=1}^N J_{ij} X_j(t - \tau_{ij}) + S(t), \quad (1)$$

where  $\tau_s$  corresponds to the synaptic time constant,  $L[u_i] = -u_i$  is a linear relaxation operator, and  $J_{ij}$  are synaptic weights. Spike trains  $X_j = \sum_{\{t_j\}} \delta(t - t_j)$  are assumed to obey non-homogeneous Poisson processes with rate  $r[u_j]$ , where  $r$  is a given sigmoidal response function [54] and  $\delta(\cdot)$  is the Dirac delta function. An additive, spatially correlated input  $S(t) = I + \sqrt{2D}\xi(t)$  is interpreted as being a functionally meaningful stimulus applied equally to all neurons, for instance resulting from coherent afferent input. This stimulus is composed of an input  $I$ , which is constant over the network and over time, and a spatially homogeneous Gaussian white noise term  $\xi(t)$  of variance  $2D$ , satisfying  $\langle \xi(t)\xi(t') \rangle = \delta(t - t')$ . Here,  $\langle \cdot \rangle$  denotes the ensemble average. Since it is additive, the stimulus  $S(t)$  does not depend on any of the system's state variables, so that  $\langle S(t) \rangle = I$ .

Equation (1) describes the dynamics of a spatially distributed network wherein neurons can either be clustered spatially (e.g., cortical microcircuit) or distant from each other (e.g., located in different brain areas). As such, the interactions within this network occur via axonal pathways which may extend globally through white matter, or alternatively locally between cortical layers, for instance. Due to this spatial separation, action potentials transit along axons of various lengths  $\ell$  with axonal conduction velocity  $c$  and thus experience a conduction delay  $\tau = \ell/c$ . The axonal conduction velocity depends on the amount of myelin covering the corresponding axon. Specifically, resulting conduction delays  $\tau_{ij} > 0$  between two neurons  $i$  and  $j$  in Eq. (1) are assumed to be random and collectively sampled from a probability distribution  $q(\tau)$  (see section below).

Under specific assumptions [21, 47, 54, 55] and whenever  $\mathbb{E}_{N,N}[J_{ij}] \equiv \bar{J} \neq 0$ , Eq. (1) admits a well defined mean field for the network ensemble average potential  $\bar{u} \equiv \mathbb{E}_N[u_i]$ . Here  $\mathbb{E}_{N,N}[J_{ij}]$  and  $\mathbb{E}_N$  are the network average across the  $N \times N$  connections and  $N$  neurons of the network, respectively. Then

$$\tau_s \frac{d}{dt} \bar{u} = L[\bar{u}] + \frac{\bar{J}}{K} \sum_{k=1}^K f[\bar{u}_{\tau_k}] + S(t) \quad (2)$$

386 for  $\bar{u}_{\tau_k} = \bar{u}(t - \tau_k)$  and conduction delay times  $\{\tau_k\}$ ,  $\tau_1 \leq \tau_2 \leq \dots \leq \tau_K$ . We  
 387 orient the reader to the Appendix and [21, 54, 55] for a thorough derivation. In this  
 388 mean field equation (2), we have introduced the network average response function  
 389  $f[\bar{u}] \equiv \mathbb{E}_N[r]$  [47, 54, 55] and expressed the sum over the  $K = N^2$  conduction delays  
 390 for notational convenience. The delay times are linked to the delay distribution by  
 391  $q(\tau) = \sum_{k=1}^K \delta(\tau - \tau_k)/K$ .

392 Equation (2) is our starting point. As defined, this mean field corresponds to a  
 393 nonlinear stochastic delay differential equation (SDDE), a well-studied [38, 40, 41,  
 394 46, 51, 52, 73], yet challenging family of dynamical systems. We are here interested in  
 395 determining the first two moments of the stationary probability density function  $\rho_S(\bar{u})$   
 396 for the mean activity  $\bar{u}$ , and how such moments depend on the delay distribution  $q(\tau)$ .  
 397 By doing so, our goal is to complement our understanding of the generic effect of delay  
 398 distribution on the dynamics of non-linear networks, and formulate conclusions about  
 399 the underlying functional role of myelin towards gain control in neural circuits.

## 400 Mean Field Moments

401 In what follows, we set the membrane time constant  $\tau_s = 1$  for simplicity and consider  
 402 a purely excitatory network, i.e.  $\bar{J} > 0$ , for which the dynamics of Eq. (2) possess  
 403 a single equilibrium. This regime holds whenever the response gain  $df/d\bar{u}$  is small,  
 404 and whenever synaptic weights  $\bar{J}$  remain below the multistability threshold. Previous  
 405 studies have successfully used approximating approaches by which the Fokker-Plank  
 406 equation for the probability density function  $\rho(\bar{u}, t)$  may be formulated in presence  
 407 of time delay, despite non-Markovian dynamics [38, 40, 41, 46]. We here opt for an  
 408 alternative (yet still approximate) strategy. We will assume that the *a priori* unknown  
 409 stationary probability density function  $\rho_S(\bar{u})$  is normally distributed with mean  $\mu_S$   
 410 and variance  $\sigma_S^2$ , that is

$$\rho_S(\bar{u}) \approx \mathcal{N}(\mu_S, \sigma_S^2) \quad (3)$$

411 This assumption implies that the stationary state of Eq. (2) in absence of noise is  
 412 non-oscillatory, and that associated eigenvalues of the corresponding linearized system  
 413 are purely real. While Eq. (2) may admit imaginary eigenvalues, this approximation  
 414 remains valid over a wide range of parameter values, and is well supported by numer-  
 415 ical observations (see Fig. 2C-D). By virtue of this Gaussian approximation, all high  
 416 order moments of  $\rho_S(\bar{u})$  vanish, and we may thus characterize the mean field  $\bar{u}$  in  
 417 Eq. (2) by developing explicit differential equations for the first and second moment,  
 418 whose fixed points correspond to the stationary statistics of  $\rho_S(\bar{u})$ .

419  
 420 The first moment, defined by

$$\mu(t) \equiv \langle \bar{u}(t) \rangle = \int_{-\infty}^{\infty} \bar{u} \rho(\bar{u}, t) d\bar{u},$$

421 is the mean potential at time  $t$ . Taking this expectation over the density of the mean  
 422 potential at time  $t$  on both sides of Eq. (2), the time-dependent mean potential  $\mu(t)$   
 423 is found to obey the following delayed (noise-free) differential equation:

$$\frac{d}{dt}\mu = L[\mu] + \frac{\bar{J}}{K} \sum_{k=1}^K \langle f[\bar{u}_{\tau_k}] \rangle + I, \quad (4)$$

424 since  $\langle S \rangle = I$ . We here introduce the expectation of the activation function  $f$

$$F[\mu, \sigma^2] \equiv \langle f[\bar{u}] \rangle = \int_{-\infty}^{\infty} f[\bar{u}] \rho(\bar{u}, t) d\bar{u}, \quad (5)$$

425 which also corresponds to the ensemble average firing rate of neurons in the network.  
 426 One may hence determine the stationary mean  $\mu_S$  through the equilibria of Eq. (4)  
 427 above, which are implicitly defined by

$$\mu_S = \bar{J}F[\mu_S, \sigma_S^2] + I. \quad (6)$$

428 Similarly, the second moment defined by

$$\langle \bar{u}^2(t) \rangle = \int_{-\infty}^{\infty} \bar{u}^2 \rho(\bar{u}, t) d\bar{u}$$

429 can be shown to obey the following differential equation [39, 41]

$$\frac{d}{dt}\langle \bar{u}^2 \rangle = 2L[\langle \bar{u}^2 \rangle] + \frac{2\bar{J}}{K} \sum_{k=1}^K \langle \bar{u} f[\bar{u}_{\tau_k}] \rangle + 2\langle \bar{u} I \rangle + 2\sqrt{2D}\langle \bar{u} \xi \rangle, \quad (7)$$

430 applying the chain rule  $\frac{d}{dt}\langle \bar{u}^2 \rangle = 2\langle \bar{u} \frac{d\bar{u}}{dt} \rangle$ . Introducing the covariance terms

$$C_k[\mu, \sigma^2] \equiv \langle \bar{u} f[\bar{u}_{\tau_k}] \rangle,$$

431 one may hence consider the equilibrium of Eq. (7) to obtain an expression for the  
 432 stationary second moment

$$\langle \bar{u}^2 \rangle_S = \frac{\bar{J}}{K} \sum_{k=1}^K C_k[\mu_S, \sigma_S^2] + \langle \bar{u} I \rangle_S + \sqrt{2D}\langle \bar{u} \xi \rangle_S \quad (8)$$

433 where the stationary average  $\langle U \rangle_S = \int U \rho_S(\bar{u}) d\bar{u}$  is performed over the stationary  
 434 probability density function  $\rho_S(\bar{u}) = \lim_{t \rightarrow \infty} \rho(\bar{u}, t)$ . The stationary value of the third  
 435 term on the right hand side of Eq.(8) may be approximated through the property of  
 436 the Ornstein-Uhlenbeck process [39]

$$\langle \bar{u} \xi \rangle_S \approx \sqrt{\frac{D}{2}}.$$

437 Since  $\sigma_S^2 = \langle \bar{u}^2 \rangle_S - \mu_S^2$  and  $\langle \bar{u} I \rangle_S = \mu_S I$ , replacing the above in Eq. (8) and  
 438 subtracting  $\mu_S^2$  on both sides gives us an implicit expression for the stationary

439 variance,

$$\sigma_S^2 = \frac{\bar{J}}{K} \sum_{k=1}^K C_k[\mu_S, \sigma_S^2] + \mu_S I + D - \mu_S^2 . \quad (9)$$

440 The covariance terms  $C_k[\mu_S, \sigma_S^2]$  correspond to the average over the stationary joint  
441 probability density function  $\rho_S(\bar{u}, \bar{u}_{\tau_k})$  [40]

$$C_k[\mu_S, \sigma_S^2] = \int_{-\infty}^{+\infty} \int_{-\infty}^{+\infty} \bar{u} f[\bar{u}_{\tau_k}] \rho_S(\bar{u}, \bar{u}_{\tau_k}) d\bar{u} d\bar{u}_{\tau_k} . \quad (10)$$

442 The above integral is to be performed over two random variables  $\bar{u}$  and  $\bar{u}_{\tau_k}$ , which are  
443 assumed to be Gaussian with mean  $\mu_S$ , variance  $\sigma_S^2$  and covariance  $\langle \bar{u} \bar{u}_{\tau_k} \rangle = \sigma_S^2 p_k$ ,  
444 where  $p_k = e^{-\gamma \tau_k}$  is the autocorrelation and  $\gamma$  is the correlation rate (see Appendix B  
445 for more details). We discuss how to determine the correlation rate in further detail  
446 in the subsequent sections below. Hence, as per Eq. (3), the joint probability density  
447 function may be written explicitly as

$$\begin{aligned} \rho_S(\bar{u}, \bar{u}_{\tau_k}) &= \rho_S(\bar{u} | \bar{u}_{\tau_k}) \rho_S(\bar{u}_{\tau_k}), \\ &= \frac{e^{-\left[ \frac{Q}{2(1-p_k^2)} - \frac{(\bar{u}_{\tau_k} - \mu_S)^2}{2\sigma_S^2} \right]}}{2\pi\sigma_S^2} \sqrt{1-p_k^2}, \end{aligned} \quad (11)$$

448 where  $Q = ((\bar{u} - \mu_S)/\sigma_S - p_k(\bar{u}_{\tau_k} - \mu_S)/\sigma_S)^2$ . Let us now examine specific examples.  
449

## 450 Linear Networks

451 To illustrate the approach above, let us first consider the simplistic case in which the  
452 response function is given by  $f[\bar{u}] = \bar{u}$  with the constant input  $I = 0$ . The mean field  
453 dynamics in Eq. (2) may be rewritten as

$$\frac{d}{dt} \bar{u} = L[\bar{u}] + \frac{\bar{J}}{K} \sum_{k=1}^K \bar{u}_{\tau_k} + \sqrt{2D} \xi(t) \quad (12)$$

454 The stationary mean  $\mu_S$ , which corresponds to the equilibrium of Eq. (12), is here  
455 given by

$$\mu_S = \bar{J} F[\mu_S, \sigma_S^2] = \bar{J} \mu_S = 0 ,$$

456 since  $\bar{J} > 0$ . Determining the variance  $\sigma_S^2$  of the stationary probability density function  
457 requires to compute the  $K$  covariance terms  $C_k[\mu_S, \sigma_S^2]$  which as per Eq. (10) simplify  
458 in the linear case to

$$C_k[\mu_S, \sigma_S^2] = \langle \bar{u} \bar{u}_{\tau_k} \rangle = \sigma_S^2 p_k = \sigma_S^2 e^{-\gamma \tau_k} .$$

459 As such, since  $\mu_S = 0$ , Eq. (9) becomes

$$\sigma_S^2 = \frac{\bar{J}\sigma_S^2}{K} \sum_{k=1}^K e^{-\gamma\tau_k} + D . \quad (13)$$

460 We note that whenever  $K \gg 1$ , the above sum can be approximated by an integral to  
461 obtain our final expression for the linear case

$$\sigma_S^2 = \bar{J}\sigma_S^2\mathcal{L}[-\gamma] + D , \quad (14)$$

462 where  $\mathcal{L}[-\gamma] = \mathbb{E}[e^{-\gamma\tau}] = \int_0^\infty e^{-\gamma\tau} q(\tau) d\tau$  is the Laplace transform of the delay prob-  
463 ability density function  $q(\tau)$ . To determine the correlation rate  $\gamma$ , we first observe  
464 that the dynamics of Eq. (12) may be well described for  $K \gg 1$  by the following  
465 Ornstein-Uhlenbeck process [41]

$$\frac{d}{dt}\bar{u} = -\alpha\bar{u} + \sqrt{2D}\xi(t) , \quad (15)$$

466 where  $\alpha = 1 - \bar{J}\mathcal{L}[-\gamma]$ . This result follows from the analysis of the characteristic  
467 equation of Eq. (12), associated with the trivial fixed point  $\bar{u}_o = 0$  in absence of noise,  
468 here given by

$$\lambda = -1 + \bar{J}\mathcal{L}[-\lambda] , \quad (16)$$

469 where  $\lambda \in \mathbb{C}$  is the eigenvalue. The eigenvalue  $\lambda$  in the equation above generically  
470 depends on both the stationary mean  $\mu_S$  and variance  $\sigma_S^2$ . However, for  $\tau_k$  small, one  
471 may consider the first order expansion [41]  $\lambda = -1 + \bar{J} + \epsilon$ ,  $\epsilon \ll 1$  in Eq. (16), for which  
472 the correlation rate becomes  $\gamma = -1 + \bar{J}$ , which we note is purely real. Substituting  
473 into Eq. (14) yields an explicit expression for the variance in the linear case i.e.,

$$\sigma_S^2 \approx \frac{D}{1 - \bar{J}\mathcal{L}[1 - \bar{J}]} = \frac{D}{\alpha} .$$

474 We note that this result corresponds to the approximation provided in previous  
475 work [41].

476

## 477 Nonlinear Networks

478 We now examine the case where the activation function in Eq. (2) is instead given by  
479 the sigmoid

$$f[\bar{u}] = \frac{1}{2} (1 + \operatorname{erf}[\beta(\bar{u} - h)]) . \quad (17)$$

480 Here,  $\beta$  is the nonlinear response gain and  $h$  the excitability threshold of the neurons.  
481 Note that Eq. (17) corresponds to the individual mean firing rate of the neurons in

482 the network, i.e.  $r_j = f[u_j]$ . In this more involved case, the stationary mean is given  
 483 by the following implicit equilibrium relationship

$$\mu_S = \bar{J}F[\mu_S, \sigma_S^2] + I, \quad (18)$$

484 where the functional  $F$  at equilibrium reflecting the ensemble average firing rate in  
 485 the network is given as per Eq. (5),

$$F[\mu_S, \sigma_S^2] = \frac{1}{2} \left( 1 + \operatorname{erf} \left[ \frac{\beta(\mu_S - h)}{\sqrt{1 + 2\beta^2\sigma_S^2}} \right] \right). \quad (19)$$

486 We note that in contrast to the linear case, now the stationary mean of  $\bar{u}$  implicitly  
 487 depends on its variance. To compute  $\sigma_S^2$ , one needs to examine the covariance terms  
 488  $C_k[\mu, \sigma^2]$  at equilibrium. Following a rather laborious technical derivation, one can  
 489 obtain

$$C_k[\mu_S, \sigma_S^2] = G[\mu_S, \sigma_S^2] \sigma_S^2 p_k + \mu_S F[\mu_S, \sigma_S^2]$$

490 with the average gain  $G$  of the network

$$G[\mu_S, \sigma_S^2] \equiv \langle f'(\bar{u}) \rangle = \int_{-\infty}^{\infty} f'(\bar{u}) \rho_S(\bar{u}) d\bar{u}. \quad (20)$$

491 This mean network gain is expressed as an average of the single neuron gain  $f'(\bar{u}) \equiv$   
 492  $df/d\bar{u}$  over the density of the average potential. This gain of the network quantifies  
 493 how the mean activity (i.e. firing rate) varies in response to changes in the mean  
 494 potential, which itself is a function of all the parameters of the system. The network  
 495 gain will be used later when gain control properties are investigated. It can be written  
 496 in terms of network parameters and  $(\mu_S, \sigma_S)$  as

$$G[\mu_S, \sigma_S^2] = \frac{\beta \exp \left[ -\frac{\beta^2(\mu_S - h)^2}{1 + 2\sigma_S^2\beta^2} \right]}{\sqrt{\pi(1 + 2\sigma_S^2\beta^2)}}. \quad (21)$$

497 Replacing into Eq. (9) yields the variance of the mean potential

$$\sigma_S^2 = \frac{\bar{J}\sigma_S^2 G[\mu_S, \sigma_S^2]}{K} \sum_{k=1}^K e^{-\gamma\tau_k} + \bar{J}\mu_S F[\mu_S, \sigma_S^2] + \mu_S I + D - \mu_S^2.$$

498 Using the fact that  $\mu_S \bar{J}F[\mu_S, \sigma_S^2] + \mu_S I = \mu_S^2$  as per Eq. (18), we may consider  $K \gg 1$   
 499 to obtain our final expression for the stationary variance in the nonlinear case

$$\sigma_S^2 = \bar{J}\sigma_S^2 G[\mu_S, \sigma_S^2] \mathcal{L}[-\gamma] + D. \quad (22)$$

500 We note that this equation together with Eq. (18) implicitly define the stationary  
 501 probability density function in Eq. (3). In other words,  $(\mu_S, \sigma_S)$  must be computed  
 502 (numerically) as the solution to these two equations. If one was to scan a parameter in

503 the model, as we do below for the noise and input strength parameters  $D$  and  $I$ , the  
 504 solution set would define a curve of such solutions in the  $(\mu_S, \sigma_S)$  space, along which  
 505 the functions  $F$  and  $G$  can be evaluated.

506 Here, the correlation rate  $\gamma$  is still undefined. As in the section above, the cor-  
 507 relation rate is also associated with the eigenvalue  $\lambda \in \mathbb{C}$  of Eq. (2), which in the  
 508 non-linear case corresponds to

$$\lambda = -1 + \bar{J}f'[\bar{u}_o]\mathcal{L}[-\lambda] ,$$

509 where the fixed point  $\bar{u}_o$  satisfies the implicit equilibrium relationship  $\bar{u}_o = \bar{J}f[\bar{u}_o] + I$   
 510 for  $D = 0$ . We here adopt the same approach as in the linear case and consider  $\tau_k$  small,  
 511 for which the first order expansion yields the real-valued eigenvalue  $\lambda \approx -1 + \bar{J}f'[\bar{u}_o] + \epsilon$   
 512 for  $\epsilon \ll 1$ , resulting in a correlation rate given by  $\gamma = -1 + \bar{J}$  to the first order.  
 513 Substituting into Eq. (22) leads to an implicit expression for the variance

$$\sigma_S^2 = \bar{J}\sigma_S^2 G[\mu_S, \sigma_S^2]\mathcal{L}[1 - \bar{J}] + D .$$

514 The above expressions for the statistics of the mean field agree well with numerical  
 515 simulations (see Fig. 3A-D).

516  
 517

## 518 Myelin and conduction delay distributions

519 To model the effect of myelin, we examined the effect of different conduction veloc-  
 520 ities  $c$  on the propagation of action potentials along axons of given lengths  $\ell$ . We  
 521 considered two specific cases, in which resulting conduction delays  $\tau = \ell/c$  adopt  
 522 different distributions:

523  
 524 **Gamma distributed delays.** Let us assume that the  $K = N^2$  axons separating  
 525 neurons in Eq. (1) possess individual lengths  $\ell_{ij}$  randomly sampled from a Gamma  
 526 distribution i.e.  $\ell_{ij} \rightarrow \Gamma[k, \theta]$ , where  $k$  and  $\theta$  refer to the shape and scale parameters,  
 527 respectively. Further, the APs propagate along those axons with constant conduction  
 528 velocity  $c$ , a value that scales with level of myelination along axons. Resulting con-  
 529 duction delays  $\tau_{ij} = \ell_{ij}/c$ , for a given conduction velocity  $c$  are hence also Gamma  
 530 distributed with density  $q(\tau) = \Gamma[k, \theta/c]$ . We point out that the mean connection  
 531 strength  $\bar{J}$  is independent of the connection topology given by the distribution of  
 532 connection lengths  $\ell_{ij}$ . In the limit of large  $N$ , the associated Laplace transform  
 533  $\mathcal{L}[-\gamma]$  is given by

$$\mathcal{L}[-\gamma] = \mathbb{E}[e^{-\gamma\tau}] = (1 + \theta\gamma/c)^{-k} .$$

534  
 535

536 **Uniformly distributed delays.** Alternatively, axons separating neurons may dis-  
 537 play individual lengths  $\ell_{ij}$  randomly sampled from a uniform distribution i.e.  $\ell_{ij} \sim$   
 538  $U[0, \ell_{\max}]$ . Then resulting conduction delays  $\tau_{ij} = \ell_{ij}/c$  are also uniformly distributed

539 with density  $q(\tau) = U[0, \ell_{\max}/c]$ . In this case, the associated Laplace transform  $\mathcal{L}[-\gamma]$   
 540 reads

$$\mathcal{L}[-\gamma] = \mathbb{E}[e^{-\gamma\tau}] = \frac{1 - e^{-\gamma\ell_{\max}/c}}{\gamma\ell_{\max}/c} .$$

### 541 Power spectral density

542 To gain better insight as to the effect of distributed delays on the response of the  
 543 network to time-varying stimuli, we computed the power spectral density  $S(\omega)$  of the  
 544 mean field  $\bar{u}$ . Specifically, we linearized Eq. (2) around the deterministic equilibrium  
 545  $\bar{u}_o$  to obtain the scalar SDDE,

$$\frac{d}{dt}\bar{u} = L[\bar{u}] + \bar{J}f'[u_o] \int_0^\infty \bar{u}(t-\tau)q(\tau)d\tau + \sqrt{2D}\xi(t) , \quad (23)$$

546 where we assumed  $K \gg 1$ . Taking the Fourier transform yields

$$i\omega\hat{u} = L[\hat{u}] + \bar{J}f'[u_o]\hat{u}\hat{q}(\omega) + \sqrt{2D}\hat{\xi}(\omega) \quad (24)$$

547 where  $\hat{u} = \hat{u}(\omega)$  and  $\hat{\xi}(\omega)$  is the Fourier transform of the mean field and the external  
 548 driving noise, respectively. Given that  $\langle \hat{\xi}(\omega)\hat{\xi}^*(\omega') \rangle = \delta(\omega - \omega')/2\pi$ , where  $*$  denotes  
 549 the complex conjugate,

$$\langle \hat{u}(\omega)\hat{u}^*(\omega') \rangle = \delta(\omega - \omega')S(\omega)$$

550 with the power spectral density

$$S(\omega) = \frac{D}{\pi (\text{Re}(P[0, \omega])^2 + \text{Im}(P[0, \omega])^2)} . \quad (25)$$

551 Here,  $\text{Re}(P[a, \omega])$  and  $\text{Im}(P[a, \omega])$  correspond to the real and imaginary parts of the  
 552 characteristic polynomial  $P[a, \omega]$  associated with the eigenvalue  $\lambda = a + i\omega \in \mathbb{C}$ ,  
 553 respectively. The polynomial  $P[a, \omega]$  associated to Eq. (23) for  $D = 0$  is given by

$$P[a, \omega] \equiv a + i\omega + 1 - Jf'[\bar{u}_o]\mathcal{L}[-\lambda] , \quad (26)$$

554 which simplifies for  $a = 0$  to

$$P[0, \omega] \equiv i\omega + 1 - Jf'[\bar{u}_o]\hat{q}(\omega) . \quad (27)$$

555 To separate the (potentially distinct) contributions of the mean delay versus delay  
 556 variance on the power spectrum in Eq. (25), we considered Gamma distributed delays  
 557 i.e.,  $q(\tau) = \Gamma(k, \theta/c)$  in the limiting case for large mean and variance. Indeed, whenever  
 558  $k \gg 1$ , the delay distribution  $q$  approaches a normal distribution i.e.  $q(\tau) \approx \mathcal{N}(m, s^2)$   
 559 with mean delay  $m = k\theta$  and variance  $s^2 = k\theta^2$ . This allows to express the Fourier  
 560 transform  $\hat{q}$  in Eq. (27) in a separable form i.e.,  $\hat{q}(\omega) = e^{-\frac{1}{2}\omega^2 s^2} e^{i\omega m}$ . We relaxed

561 the premises above, and assumed that the mean delay  $m$  and variance  $s^2$  may be  
562 modulated independently in a regime where  $m > s$ . While this clearly does not hold  
563 for the Gamma distributed case (since the mean and variance are not independent),  
564 this approach remains insightful for delay distributions, that adopt a Gaussian shaped  
565 profile. We note, that one may alternatively consider uniformly distributed delays  
566 within the interval  $[m - \delta\tau, m + \delta\tau]$ , in which case the delay distribution adopts a  
567 mean  $m$  and variance  $s^2 = 3\delta\tau^2$  instead. This yields qualitatively similar results as  
568 those portrayed in Fig 5.

## 569 **Declarations**

### 570 **Funding**

571 We thank the National Sciences and Engineering Research Council of Canada (NSERC  
572 Grants RGPIN-2017-06662) for support of this research.

### 573 **Data availability**

574 The data, algorithms and numerical methods that support the findings of this study  
575 are available from the corresponding author upon reasonable request.

### 576 **Author contribution**

577 J.L. designed the study. A.C. provided support for the simulations. J.L., A.H. and  
578 A.L. performed the analysis and wrote the manuscript.

## 579 **Appendix A Mean Field Derivation**

580 The evolution equation (1) describes how the activity of single neurons evolve on short  
581 time scales. This short time scale is observed by the neurons' spike-coupling. The  
582 equation can be written as

$$\tau_s \frac{d}{dt} u_i = L[u_i] + I_i + \sqrt{2D}\xi(t) \quad (\text{A1})$$

583 with

$$\begin{aligned} I_i &= \frac{1}{N} \sum_{j=1}^N J_{ij} X_j(t - \tau_{ij}) \\ &= \frac{1}{N} \int_0^\infty dT \sum_{j=1}^N J_{ij} \delta(T - \tau_{ij}) X_j(t - T) . \end{aligned}$$

584 Let us consider the eigenvalue spectrum of the connectivity matrix  $\mathbf{J}$  [47] with the  
585 basis vectors  $\{\psi_j\}$ ,  $\{\phi_i\}$ ,  $\psi_j, \phi_j \in \mathcal{C}^N$  and the eigenvalues  $\lambda_j \in \mathcal{C}$ , which obey

$$\psi_j^\dagger \phi_i = \delta_{ji}$$

$$\psi_j^\dagger \mathbf{J} = \lambda_j \psi_j^\dagger.$$

586 Here,  $\dagger$  denotes the complex conjugate transposition and  $\delta_{ji}$  is the Kronecker symbol  
 587 with  $\delta_{ii} = 1$  and  $\delta_{ij} = 0$ ,  $i \neq j$ . Then

$$\psi_k^\dagger \mathbf{I} = \frac{1}{N} \int_0^\infty dT \sum_{i=1}^N \sum_{j=1}^N (\psi_k^\dagger)_i J_{ij} \delta(T - \tau_{ij}) X_j(t - T) \quad (\text{A2})$$

588 and

$$\begin{aligned} & \sum_{i=1}^N (\psi_k^\dagger)_i J_{ij} \delta(T - \tau_{ij}) \\ &= N \frac{1}{N} \sum_{i=1}^N (\psi_k^\dagger)_i J_{ij} \delta(T - \tau_{ij}) \\ &= N \left( \frac{1}{N} \sum_{i=1}^N (\psi_k^\dagger)_i J_{ij} \right) \left( \frac{1}{N} \sum_{i=1}^N \delta(T - \tau_{ij}) \right) + \varepsilon_j \end{aligned} \quad (\text{A3})$$

$$= \lambda_k (\psi_k^\dagger)_j \left( \int_0^\infty \delta(T - x_j) p_j^\tau(x_j) dx_j + \varepsilon_j^\tau \right) + \varepsilon_j \quad (\text{A4})$$

$$\begin{aligned} &= \lambda_k (\psi_k^\dagger)_j (p_j^\tau(T) + \varepsilon_j^\tau) + \varepsilon_j \\ &\approx \lambda_k (\psi_k^\dagger)_j p_j^\tau(T). \end{aligned} \quad (\text{A5})$$

589 The terms  $\varepsilon_j$  denote the error of the approximation  $E[XY] \approx E[X]E[Y]$  applied in  
 590 Eq. (A3) and  $\varepsilon_j^\tau$  represents the approximation error made by replacing the finite sum  
 591 by an integral in Eq. (A4) [47]. Both error terms vanish for infinite networks, i.e.  
 592  $N \rightarrow \infty$ , yielding Eq. (A5). The term  $p_j^\tau(T)$  denotes the probability density function  
 593 of the conduction delays  $\tau_{ij}$  in connections to the node  $j$ .

594 Inserting Eq. (A5) into Eq. (A2) yields

$$\begin{aligned} \psi_k^\dagger \mathbf{I} &= \frac{\lambda_k}{N} \int_0^\infty dT \sum_{j=1}^N (\psi_k^\dagger)_j p_j^\tau(T) X_j(t - T) \\ &\approx \frac{\lambda_k}{N} \int_0^\infty dT \left( \frac{1}{N} \sum_{j=1}^N (\psi_k^\dagger)_j \right) \times \\ &\quad \left( \frac{1}{N} \sum_{j=1}^N X_j(t - T) \right) q(T) \\ &= \frac{\lambda_k \bar{\psi}_k}{N} \int_0^\infty dT \bar{X}(t - T) q(T), \end{aligned} \quad (\text{A6})$$

595 where we assumed homogeneous conduction delays with  $p_j^\tau(x) = q(x)$  and we approx-  
 596 imated the network mean over  $\psi_k$  and  $X_j(t - T)$  by the product of their respective  
 597 mean values  $\bar{\psi}_k$  and  $\bar{X}(t - T)$ . This approximation holds well for large networks.  
 598 Multiplying Eq. (A1) by  $(\psi_k^\dagger)_i$ , taking the corresponding sum and inserting Eq. (A6)  
 599 leads to

$$\tau_s \frac{d}{dt} \psi_k^\dagger \mathbf{u}(t) = L[\psi_k^\dagger \mathbf{u}] + \frac{\lambda_k \bar{\psi}_k}{N} \int_0^\infty dT \bar{X}(t - T) q(T) + \sqrt{2D} \psi_k^\dagger \xi(t)$$

600 It can be shown [47, 74], that imbalanced infinite Erdos-Renyi networks can be  
 601 chosen to have an edge spectrum with a single eigenvalue  $\lambda_1$  and the eigenvector  
 602  $\psi_1 = (1/N, \dots, 1/N)^t$  and a vanishing bulk spectrum. Then for  $k = 1$

$$\tau_s \frac{d}{dt} U(t) = L[U] + \frac{\lambda_1}{N^2} \int_0^\infty dT \bar{X}(t - T) q(T) + \sqrt{2D} \bar{\xi}(t)$$

603 with  $U(t) = \psi_1^\dagger \mathbf{u}(t)$ . If the synaptic time constant  $\tau_s$  is large, i.e. tens of milliseconds,  
 604 then the equation considers slow synaptic response activity  $U(t)$  and fast incoming  
 605  $\delta$ -function-like spike trains (included in  $\bar{X}(t)$ ). Now choosing the slow time scale as  
 606 the primary scale of description of the network's dynamics, we average the system  
 607 activity over a short time window  $\Delta t$  with

$$\bar{u}(t) = \frac{1}{\Delta t} \int_{t-\Delta t}^t U(t') dt'$$

608 yielding

$$\tau_s \frac{d}{dt} \bar{u}(t) = L[\bar{u}] + \frac{\lambda_1}{N^2} \int_0^\infty dT f[\bar{u}(t - T)] q(T) + \sqrt{2D} \bar{\xi}(t) .$$

609 Here,

$$\begin{aligned} f[x(t)] &= \frac{1}{N} \sum_{j=1}^N \int_{t-\Delta t}^t \frac{X_j(t')}{\Delta t} dt' \\ &= \frac{1}{N} \sum_{j=1}^N M_j[\bar{u}(t)], \end{aligned}$$

610 where the last equation assumes asynchronous neural activity in the population in  
 611 line with previous studies [69, 75] and  $M_j$  is the number of spikes at neuron  $j$  in the  
 612 time interval  $[t - \Delta t; t]$ .

613 Since the delay times  $\tau_{ij}$  of number  $K = N^2$  are discrete values, we can write

$$q(T) = \frac{1}{K} \sum_{k=1}^K \delta(T - \tau_k),$$

614 which leads to the final equation (2) with  $\bar{J} = \lambda_1/K$ .

## 615 Appendix B Stationary conditional probability 616 density

617 We assume two random normal distributed variables  $X$  and  $Y$ , which are correlated  
618 with the correlation function  $\sigma_{XY}^2$ . Then the conditional probability density function  
619  $p(y|x)$  is also normal distributed with

$$p(y|x) = \frac{1}{\sqrt{2\pi}\sigma_{y|x}^2} e^{-(y-\mu_{y|x})^2/2\sigma_{y|x}^2} \quad (\text{B7})$$

620 with mean  $\mu_{y|x}$  and variance  $\sigma_{y|x}^2$ .

621 Moreover, we assume that there is some kind of linear relationship between  $X$  and  $Y$ .

622 This leads to the linear ansatz

$$\mu_{y|x} = \mu_y + \rho \frac{\sigma_y}{\sigma_x} (x - \mu_x) \quad (\text{B8})$$

623 with the mean value  $\mu_x, \mu_y$  and variance  $\sigma_x^2, \sigma_y^2$  of  $X, Y$  accompanied by the variance

$$\sigma_{y|x}^2 = \sigma_y^2 (1 - \sigma_{XY}^2). \quad (\text{B9})$$

624 Inserting Eq. (B8) and (B9) into Eq. (B7) yields the conditional probability density  
625 function.

626 In the context of Eqs. (10) and (11),  $\mu_x = \mu_y = \mu_s$ ,  $\sigma_x = \sigma_y = \sigma_s$ ,  $Y = \bar{u}$ ,  $X = \bar{u}_\tau$  we  
627 gain  $\rho_s(\bar{u}|\bar{u}_\tau) = p(y|x)$ . The correlation function is

$$\sigma_{XY}^2 = \frac{E[\bar{u}(t)\bar{u}(t - \tau_k)]}{\sigma_s^2}.$$

## 628 References

- 629 [1] Buldú, J.M., Garcia-Ojalvo, J., Torrent, M.C.: Delay-induced resonances in an  
630 optical system with feedback. Phys. Rev. E **69**(4), 046207 (2004) [https://doi.org/  
631 10.1103/PhysRevE.69.046207](https://doi.org/10.1103/PhysRevE.69.046207)
- 632 [2] Eurich, C.W., Milton, J.G.: Noise-induced transitions in human postural sway.  
633 Phys. Rev. E **54**(6), 6681 (1996) <https://doi.org/10.1103/PhysRevE.54.6681>
- 634 [3] Erneux, T.: Applied Delay Differential Equations. Springer, Heidelberg (2009)

- 635 [4] Hutt, A., Bestehorn, M., Wennekers, T.: Pattern formation in intracortical neuronal fields. *Network: Comput. Neural Syst.* **14**, 351–368 (2003) <https://doi.org/10.1088/0954-898X-14.2.310>
- 636
- 637
- 638 [5] Hutt, A., Rougier, N.: Activity spread and breathers induced by finite transmission speeds in two-dimensional neural fields. *Phys. Rev. E* **82**, 055701 (2010) <https://doi.org/10.1103/PhysRevE.82.055701>
- 639
- 640
- 641 [6] Liu, C., Wang, J., Yu, H., Deng, B., Tsang, K.M., Chan, W.L., Wong, Y.K.: The effects of time delay on the stochastic resonance in feed-forward-loop neuronal network motifs. *Comm. Nonlin. Sci. Num. Sim.* **19**(4), 1088–1096 (2014) <https://doi.org/10.1016/j.cnsns.2013.08.021>
- 642
- 643
- 644
- 645 [7] Hashemi, M., Hutt, A., Hight, D., Sleigh, J.: Anesthetic action on the transmission delay between cortex and thalamus explains the beta buzz observed under propofol anesthesia. *PLoS* **12**(6), 0179286 (2017) <https://doi.org/10.1371/journal.pone.0179286>
- 646
- 647
- 648
- 649 [8] Choi, M.Y., Kim, H.J., Kim, D., Hong, H.: Synchronization in a system of globally coupled oscillators with time delay. *Phys. Rev. E* **61**(4), 371 (2000) <https://doi.org/10.1103/PhysRevE.61.371>
- 650
- 651
- 652 [9] Dhamala, M., Jirsa, V.K., Ding, M.: Enhancement of neural synchrony by time delay. *Phys. Rev. Lett.* **92**(7), 074104 (2004) <https://doi.org/10.1103/PhysRevLett.92.074104>
- 653
- 654
- 655 [10] Sen, M.K., Bag, B.C., Petrosyan, K.G., Hu, C.-K.: Effect of time delay on the onset of synchronization of the stochastic kuramoto model. *J. Stat. Mech.*, 08018 (2010) <https://doi.org/10.1088/1742-5468/2010/08/P08018>
- 656
- 657
- 658 [11] Ray, S., Sen, M.K., Baura, A., Bag, B.C.: Lifetime of the incoherent state of coupled phase oscillators. *Eur. Phys. J. B* **85**(11), 306 (2012) <https://doi.org/10.1140/epjb/e2012-30412-8>
- 659
- 660
- 661 [12] Deco, G., Jirsa, V., McIntosh, A.R., Sporns, O., Kötter, R.: Key role of coupling, delay, and noise in resting brain fluctuations. *Proc. Natl. Acad. Sci. USA* **106**(25), 10302–10307 (2009) <https://doi.org/10.1073/pnas.0901831106>
- 662
- 663
- 664 [13] Noori, R., Park, D., Griffiths, J.D., Bells, S., Frankland, P.W., Mabbott, D., Lefebvre, J.: Activity-dependent myelination: A glial mechanism of oscillatory self-organization in large-scale brain networks. *Proc. Natl. Acad. Sci. USA* **117**(24), 13227–13237 (2020) <https://doi.org/10.1073/pnas.1916646117>
- 665
- 666
- 667
- 668 [14] Roxin, A., Brunel, N., Hansel, D.: Role of delays in shaping spatiotemporal dynamics of neuronal activity in large networks. *Phys. Rev. Lett.* **94**, 238103 (2005) <https://doi.org/10.1103/PhysRevLett.94.238103>
- 669
- 670

- 671 [15] Deco, G., Jirsa, V.K., Robinson, P.A., Breakspear, M., Friston, K.: The dynamic  
672 brain: from spiking neurons to neural masses and cortical fields. *PLoS Comput.*  
673 *Biol.* **4**(8), 1000092 (2008) <https://doi.org/10.1371/journal.pcbi.1000092>
- 674 [16] Cabral, J., Castaldo, F., Vohryzek, J., Litvak, V., Bick, C., Lambiotte, R., Fris-  
675 ton, K., Kringelbach, M.L., Deco, G.: Metastable oscillatory modes emerge from  
676 synchronization in the brain spacetime connectome. *Commun. Phys.* **5**(1), 184  
677 (2022) <https://doi.org/10.1038/s42005-022-00950-y>
- 678 [17] Salami, M., Itami, C., Tsumoto, T., Kimura, F.: Change of conduction velocity  
679 by regional myelination yields constant latency irrespective of distance between  
680 thalamus and cortex. *Proceed. Natl. Acad. Sci.* **100**(10), 6174–6179 (2003) <https://doi.org/10.1073/pnas.09373801>
- 682 [18] Swadlow, H.A., Rosene, D.L., Waxman, S.G.: Characteristics of interhemispheric  
683 impulse conduction between prelunate gyri of the rhesus monkey. *Exp. Brain Res.*  
684 **33**, 455–467 (1978) <https://doi.org/10.1007/BF00235567>
- 685 [19] Swadlow, H.A., Waxman, S.G.: Axonal conduction delays. *Scholarpedia* **7**(6),  
686 1451 (2012) <https://doi.org/10.4249/scholarpedia.1451>
- 687 [20] Doiron, B., Litwin-Kumar, A., Rosenbaum, R., Ocker, G.K., Josić, K.: The me-  
688 chanics of state-dependent neural correlations. *Nature Neurosci.* **19**(3), 383–393  
689 (2016) <https://doi.org/10.1038/nn.4242>
- 690 [21] Talidou, A., Frankland, P.W., Mabbott, D., Lefebvre, J.: Homeostatic co-  
691 ordination and up-regulation of neural activity by activity-dependent myeli-  
692 nation. *Nature Comput. Sci.* **2**(10), 665–676 (2022) <https://doi.org/10.1038/s43588-022-00315-z>
- 694 [22] Shadlen, M.N., Newsome, W.T.: The variable discharge of cortical neurons: im-  
695 plications for connectivity, computation, and information coding. *J. Neurosci.*  
696 **18**(10), 3870–3896 (1998) <https://doi.org/10.1523/JNEUROSCI.18-10-03870.1998>
- 698 [23] Izhikevich, E.M.: Polychronization: computation with spikes. *Neural Comput.*  
699 **18**(2), 245–282 (2006) <https://doi.org/10.1162/089976606775093882>
- 700 [24] Gibson, E.M., Purger, D., Mount, C.W., Goldstein, A.K., Lin, G.L., Wood,  
701 L.S., Inema, I., Miller, S.E., Bieri, G., Zuchero, J.B., Barres, B.A., Woo, P.J.,  
702 Vogel, H., Monje, M.: Neuronal activity promotes oligodendrogenesis and adap-  
703 tive myelination in the mammalian brain. *Science* **344**(6183), 1252304 (2014)  
704 <https://doi.org/10.1126/science.1252304>
- 705 [25] Auer, F., Vagionitis, S., Czopka, T.: Evidence for myelin sheath remodeling in  
706 the CNS revealed by in vivo imaging. *Curr. Biol.* **28**(4), 549–559 (2018) <https://doi.org/10.1038/s41593-018-0121-5>
- 707

- 708 [26] Mount, C.W., Monje, M.: Wrapped to adapt: experience-dependent myelination.  
709 *Neuron* **95**(4), 743–756 (2017) <https://doi.org/10.1016/j.neuron.2017.07.009>
- 710 [27] Fields, R.D.: A new mechanism of nervous system plasticity: activity-dependent  
711 myelination. *Nature Rev. Neurosci.* **16**(12), 756–767 (2015) <https://doi.org/10.1038/nrn4023>  
712
- 713 [28] Steadman, P.E., Xia, F., Ahmed, M., Mocle, A.J., Penning, A.R.A., Geraghty,  
714 A.C., Steenland, H.W., Monje, M., Josselyn, S.A., Frankland, P.W.: Disruption of  
715 oligodendrogenesis impairs memory consolidation in adult mice. *Neuron* **105**(1),  
716 150–164 (2020) <https://doi.org/10.1016/j.neuron.2019.10.013>
- 717 [29] Fields, R.D., Bukalo, O.: Myelin makes memories. *Nature Neurosci.* **23**(4), 469–  
718 470 (2020) <https://doi.org/10.1038/s41593-020-0606-x>
- 719 [30] Xin, W., Chan, J.R.: Myelin plasticity: sculpting circuits in learning and mem-  
720 ory. *Nature Rev. Neurosci.* **21**(12), 682–694 (2020) <https://doi.org/10.1038/s41583-020-00379-8>  
721
- 722 [31] Cheng, S.-M., Carr, C.E.: Functional delay of myelination of auditory delay lines  
723 in the nucleus laminaris of the barn owl. *Develop. Neurobiol.* **67**(14), 1957–1974  
724 (2007) <https://doi.org/10.1002/dneu.20541>
- 725 [32] Bells, S., Lefebvre, J., Prescott, S.A., Dockstader, C., Bouffet, E., Skocic, J.,  
726 Laughlin, S., Mabbott, D.J.: Changes in white matter microstructure impact cog-  
727 nition by disrupting the ability of neural assemblies to synchronize. *J. Neurosci.*  
728 **37**(34), 8227–8238 (2017) <https://doi.org/10.1523/JNEUROSCI.0560-17.2017>
- 729 [33] Bells, S., Lefebvre, J., Longoni, G., Narayanan, S., Arnold, D.L., Yeh, E.A., Mab-  
730 bott, D.J.: White matter plasticity and maturation in human cognition. *Glia*  
731 **67**(11), 2020–2037 (2019) <https://doi.org/10.1002/glia.23661>
- 732 [34] Nature Neuroscience: Glia move to the foreground. *Nature Neuroscience* **27**(8),  
733 1427–1427 (2024) <https://doi.org/10.1038/s41593-024-01735-y>
- 734 [35] Ferraina, S., Paré, M., Wurtz, R.H.: Comparison of cortico-cortical and cortico-  
735 collicular signals for the generation of saccadic eye movements. *Journal of*  
736 *neurophysiology* **87**(2), 845–858 (2002) <https://doi.org/10.1152/jn.00317.2001>
- 737 [36] Swadlow, H.A.: Efferent neurons and suspected interneurons in s-1 forelimb rep-  
738 resentation of the awake rabbit: receptive fields and axonal properties. *Journal*  
739 *of Neurophysiology* **63**(6), 1477–1498 (1990) <https://doi.org/10.1152/jn.1990.63.6.1477>  
740
- 741 [37] Horsthemke, W., Lefever, R.: Noise-Induced Transitions: Theory and Applica-  
742 tions in Physics, Chemistry, and Biology. Springer Series in Synergetics, vol. 15.  
743 Springer, Heidelberg (1984). <https://doi.org/10.1007/978-3-642-69689-3>

- 744 [38] Frank, T.D., Beek, P.J.: Stationary solutions of linear stochastic delay differential  
745 equations: Applications to biological systems. *Phys. Rev. E* **64**(2), 021917 (2001)  
746 <https://doi.org/10.1103/PhysRevE.64.021917>
- 747 [39] Frank, T.D., Beek, P.J., Friedrich, R.: Fokker-Planck perspective on stochastic  
748 delay systems: Exact solutions and data analysis of biological systems. *Phys. Rev.*  
749 *E* **68**(2), 021912 (2003) <https://doi.org/10.1103/PhysRevE.68.021912>
- 750 [40] Frank, T.D.: Delay Fokker-Planck equations, perturbation theory, and data anal-  
751 ysis for nonlinear stochastic systems with time delays. *Phys. Rev. E* **71**(3), 031106  
752 (2005) <https://doi.org/10.1103/PhysRevE.71.031106>
- 753 [41] Frank, T.D.: Kramers–Moyal expansion for stochastic differential equations with  
754 single and multiple delays: Applications to financial physics and neurophysics.  
755 *Phys. Lett. A* **360**(4-5), 552–562 (2007) [https://doi.org/10.1016/j.physleta.2006.](https://doi.org/10.1016/j.physleta.2006.08.062)  
756 [08.062](https://doi.org/10.1016/j.physleta.2006.08.062)
- 757 [42] Pajevic, S., Plenz, D., Basser, P.J., Fields, R.D.: Oligodendrocyte-mediated  
758 myelin plasticity and its role in neural synchronization. *eLife* **12**, 81982 (2023)  
759 <https://doi.org/10.7554/eLife.81982>
- 760 [43] Knowles, J.K., Xu, H., Soane, C., Batra, A., Saucedo, T., Frost, E., Tam, L.T.,  
761 Fraga, D., Ni, L., Villar, K., Talmi, S., Huguenard, J.R., Monje, M.: Maladaptive  
762 myelination promotes generalized epilepsy progression. *Nature Neurosci.* **25**(5),  
763 596–606 (2022) <https://doi.org/10.1038/s41593-022-01052-2>
- 764 [44] Rahmzadeh, R., Lu, P.-J., Barakovic, M., Weigel, M., Maggi, P., Nguyen,  
765 T.D., Schiavi, S., Daducci, A., La Rosa, F., Schaedelin, S., Absinta, M., Reich,  
766 D.S., Sati, P., Wang, Y., Bach Cuadra, M., Radue, E.-W., Kuhle, J., Kappos,  
767 L., Granziera, C.: Myelin and axon pathology in multiple sclerosis assessed by  
768 myelin water and multi-shell diffusion imaging. *Brain* **144**(6), 1684–1696 (2021)  
769 <https://doi.org/10.1093/brain/awab088>
- 770 [45] Lam, S.K., Pitrou, A., Seibert, S.: Numba: a llvm-based python jit compiler. In:  
771 Proceedings of the Second Workshop on the LLVM Compiler Infrastructure in  
772 HPC. LLVM '15. Association for Computing Machinery, New York, NY, USA  
773 (2015). <https://doi.org/10.1145/2833157.2833162>
- 774 [46] Guillouzic, S., L’Heureux, I., Longtin, A.: Small delay approximation of stochastic  
775 delay differential equations. *Phys. Rev. E* **59**(4), 3970 (1999) [https://doi.org/10.](https://doi.org/10.1103/PhysRevE.59.3970)  
776 [1103/PhysRevE.59.3970](https://doi.org/10.1103/PhysRevE.59.3970)
- 777 [47] Lefebvre, J., Hutt, A.: Induced synchronization by endogenous noise modula-  
778 tion in finite-size random neural networks: A stochastic mean-field study. *Chaos*  
779 **33**(12), 123110 (2023) <https://doi.org/10.1063/5.0167771>
- 780 [48] Atay, F.M.: Distributed delays facilitate amplitude death of coupled oscillators.

- 781 Physical Rev. Lett. **91**(9), 094101 (2003) [https://doi.org/10.1103/PhysRevLett.](https://doi.org/10.1103/PhysRevLett.91.094101)  
782 [91.094101](https://doi.org/10.1103/PhysRevLett.91.094101)
- 783 [49] Meyer, U., Shao, J., Chakrabarty, S., Brandt, S.F., Luksch, H., Wessel, R.: Dis-  
784 tributed delays stabilize neural feedback systems. *Biol. Cybern.* **99**, 79–87 (2008)  
785 <https://doi.org/10.1007/s00422-008-0239-8>
- 786 [50] Tavakoli, S.K., Longtin, A.: Multi-delay complexity collapse. *Phys. Rev. Res.*  
787 **2**(3), 033485 (2020) <https://doi.org/10.1103/PhysRevResearch.2.033485>
- 788 [51] Hutt, A., Lefebvre, J., Longtin, A.: Delay stabilizes stochastic systems near a  
789 non-oscillatory instability. *Europhys. Lett.* **98**(2), 20004 (2012) [https://doi.org/](https://doi.org/10.1209/0295-5075/98/20004)  
790 [10.1209/0295-5075/98/20004](https://doi.org/10.1209/0295-5075/98/20004)
- 791 [52] Lefebvre, J., Hutt, A.: Additive noise quenches delay-induced oscillations. *Euro-*  
792 *phys. Lett.* **102**(6), 60003 (2013) <https://doi.org/10.1209/0295-5075/102/60003>
- 793 [53] Naud, R., Longtin, A.: Spike-diffuse-spike model of axonal propagation links de-  
794 myelination to compound action potential dispersion. *J. Math. Neurosci.* **9**, 3  
795 (2019) <https://doi.org/10.1186/s13408-019-0071-6>
- 796 [54] Hutt, A., Mierau, A., Lefebvre, J.: Dynamic control of synchronous activity in  
797 networks of spiking neurons. *PloS One* **11**(9), 0161488 (2016) [https://doi.org/10.](https://doi.org/10.1371/journal.pone.0161488)  
798 [1371/journal.pone.0161488](https://doi.org/10.1371/journal.pone.0161488)
- 799 [55] Lefebvre, J., Hutt, A., Knebel, J.-F., Whittingstall, K., Murray, M.M.: Stimulus  
800 statistics shape oscillations in nonlinear recurrent neural networks. *J. Neurosci.*  
801 **35**(7), 2895–2903 (2015) <https://doi.org/10.1523/JNEUROSCI.3609-14.2015>
- 802 [56] Hutt, A., Lefebvre, J., Hight, D., Kaiser, H.A.: Phase coherence induced by ad-  
803 ditive Gaussian and non-Gaussian noise in excitable networks with application  
804 to burst suppression-like brain signals. *Front. Appl. Math. Stat.* **5**, 69 (2020)  
805 <https://doi.org/10.3389/fams.2019.00069>
- 806 [57] Lim, S., McKee, J.L., Woloszyn, L., Amit, Y., Freedman, D.J., Sheinberg, D.L.,  
807 Brunel, N.: Inferring learning rules from distributions of firing rates in cortical  
808 neurons. *Nature Neurosci.* **18**, 1804–1810 (2015) [https://doi.org/10.1038/nn.](https://doi.org/10.1038/nn.4158)  
809 [4158](https://doi.org/10.1038/nn.4158)
- 810 [58] Ly, C., Marsat, G.: Variable synaptic strengths controls the firing rate distribution  
811 in feedforward neural networks. *J. Comput. Neurosci.* **44**, 75–95 (2018) [https:](https://doi.org/10.1007/s10827-017-0670-8)  
812 [//doi.org/10.1007/s10827-017-0670-8](https://doi.org/10.1007/s10827-017-0670-8)
- 813 [59] Williamson, J.M., Lyons, D.A.: Myelin dynamics throughout life: an ever-  
814 changing landscape ? *Front. Cell. Neurosci.* **12**, 424 (2018) [https://doi.org/10.](https://doi.org/10.3389/fncel.2018.00424)  
815 [3389/fncel.2018.00424](https://doi.org/10.3389/fncel.2018.00424)

- 816 [60] Allen, N.J., Lyons, D.A.: Glia as architects of central nervous system formation  
817 and function. *Science* **362**(6411), 181–185 (2018) <https://doi.org/10.1126/science.aat0473>  
818
- 819 [61] Suminaite, D., Lyons, D.A., Livesey, M.R.: Myelinated axon physiology and reg-  
820 ulation of neural circuit function. *Glia* **67**(11), 2050–2062 (2019) <https://doi.org/10.1002/glia.23665>  
821
- 822 [62] Seidl, A.H.: Regulation of conduction time along axons. *Neuroscience* **276**, 126–  
823 134 (2014) <https://doi.org/10.1016/j.neuroscience.2013.06.047>
- 824 [63] Jasper, H.H.: *Jasper’s Basic Mechanisms of the Epilepsies* vol. 80. OUP USA,  
825 Bethesda (MD) (2012)
- 826 [64] Bacmeister, C.M., Huang, R., Osso, L.A., Thornton, M.A., Conant, L., Chavez,  
827 A.R., Poleg-Polsky, A., Hughes, E.G.: Motor learning drives dynamic patterns of  
828 intermittent myelination on learning-activated axons. *Nature Neurosci.* **25**(10),  
829 1300–1313 (2022) <https://doi.org/10.1038/s41593-022-01169-4>
- 830 [65] Pan, S., Mayoral, S.R., Choi, H.S., Chan, J.R., Kheirbek, M.A.: Preservation of  
831 a remote fear memory requires new myelin formation. *Nature Neurosci.* **23**(4),  
832 487–499 (2020) <https://doi.org/10.1038/s41593-019-0582-1>
- 833 [66] Kohama, S.G., Rosene, D.L., Sherman, L.S.: Age-related changes in human and  
834 non-human primate white matter: from myelination disturbances to cognitive  
835 decline. *Age* **34**, 1093–1110 (2012) <https://doi.org/10.1007/s11357-011-9357-7>
- 836 [67] Wang, F., Ren, S.-Y., Chen, J.-F., Liu, K., Li, R.-X., Li, Z.-F., Hu, B., Niu, J.-Q.,  
837 Xiao, L., Chan, J.R., Mei, F.: Myelin degeneration and diminished myelin renewal  
838 contribute to age-related deficits in memory. *Nature Neurosci.* **23**(4), 481–486  
839 (2020) <https://doi.org/10.1038/s41593-020-0588-8>
- 840 [68] Dumont, G., Northoff, G., Longtin, A.: Linear noise approximation for oscillations  
841 in a stochastic inhibitory network with delay. *Phys. Rev. E* **90**, 012702 (2014)  
842 <https://doi.org/10.1103/PhysRevE.90.012702>
- 843 [69] Brunel, N., Hakim, V.: Fast global oscillations in networks of integrate-and-fire  
844 neurons with low firing rates. *Neural Comput.* **11**, 1621–1671 (1999) <https://doi.org/10.1162/089976699300016179>  
845
- 846 [70] Doiron, B., Lindner, B., Longtin, A., Maler, L., Bastian, J.: Oscillatory activity  
847 in electrosensory neurons increases with the spatial correlation of the stochastic  
848 input stimulus. *Phys. Rev. Lett.* **93**, 048101 (2004) <https://doi.org/10.1103/PhysRevLett.93.048101>  
849
- 850 [71] Yang, S.M., Michel, K., Jokhi, V., Nedivi, E., Arlotta, P.: Neuron class-specific  
851 responses govern adaptive myelin remodeling in the neocortex. *Science* **370**(6523),

- 852 2109 (2020) <https://doi.org/10.1126/science.abd2109>
- 853 [72] Call, C.L., Bergles, D.E.: Cortical neurons exhibit diverse myelination patterns  
854 that scale between mouse brain regions and regenerate after demyelination. *Nat.*  
855 *Commun.* **12**(1), 1–15 (2021) <https://doi.org/10.1038/s41467-021-25035-2>
- 856 [73] René, A., Longtin, A.: Mean, covariance, and effective dimension of stochas-  
857 tic distributed delay dynamics. *Chaos* **27**(11) (2017) [https://doi.org/10.1063/1.](https://doi.org/10.1063/1.5007866)  
858 [5007866](https://doi.org/10.1063/1.5007866)
- 859 [74] Hutt, A., Wahl, T., Voges, N., Hausmann, J., Lefebvre, J.: Coherence resonance  
860 in random Erdos-Renyi neural networks : mean-field theory. *Front. Appl. Math.*  
861 *Stat.* **7**, 697904 (2021) <https://doi.org/10.3389/fams.2021.697904>
- 862 [75] Brunel, N.: Dynamics of sparsely connected networks of excitatory and inhibitory  
863 spiking neurons. *J. Comput. Neurosci.* **8**, 183–208 (2000) [https://doi.org/10.](https://doi.org/10.1023/A:1008925309027)  
864 [1023/A:1008925309027](https://doi.org/10.1023/A:1008925309027)